Virologica Sinica 40 (2025) 361–373

Contents lists available at ScienceDirect

Virologica Sinica

journal homepage: www.keaipublishing.com/en/journals/virologica-sinica
www.virosin.org

Research Article

# Elevated interferon-induced transmembrane protein 3 in platelets and megakaryocytes suppresses Crimean-Congo hemorrhagic fever viral infection by interacting with glycoprotein Gc

Jingyuan Zhang [a,b,1], Yaohui Fang [a,b,1], Chenhui Lin [a,b], Xiaoli Wu [a], Chaoxiong Yue [a], Fei Deng [a,*], Shu Shen [a,c,*]

[a] Key Laboratory of Virology and Biosafety and National Virus Resource Center, Wuhan Institute of Virology, Chinese Academy of Sciences, Wuhan, 430070, China
[b] University of Chinese Academy of Sciences, Beijing, 100049, China
[c] Xinjiang Key Laboratory of Vector-borne Infectious Diseases, Urumqi, 830002, China

ARTICLE INFO

*Keywords:*
Crimean-Congo hemorrhagic fever virus (CCHFV)
Interferon-induced transmembrane protein 3 (IFITM3)
Platelet
Megakaryocytes

ABSTRACT

Crimean-Congo hemorrhagic fever (CCHF) is a hemorrhagic fever caused by infection with the CCHF virus (CCHFV) and has a mortality rate of up to 30 %. Thrombocytopenia is a hallmark of CCHF; however, the mechanisms underlying this manifestation remain poorly understood. In addition to hemostasis, platelets play a crucial role in recognizing pathogens and mediating immune responses. We investigated the mechanisms underlying thrombocytopenia associated with CCHFV infection by analyzing the platelet transcriptome in mice. Interferon-induced transmembrane protein 3 (IFITM3), a known antiviral factor, was significantly upregulated. The role of IFITM3 in response to CCHFV infection was characterized using the human megakaryoblast cell line MEG-01, considered a parental cell line of platelets. Although the CCHFV infection rate was limited, MEG-01 cells maintained the infection and replication of CCHFV, leading to increased IFITM3 protein expression. We demonstrated that IFITM3 overexpression efficiently inhibited CCHFV infection, whereas IFITM3 knockout promoted viral infection. An interaction between IFITM3 and the CCHFV glycoprotein Gc was identified, which suppressed CCHFV entry into cells. The IFITM3 CIL-TMD domain is critical for this interaction. These results suggest that IFITM3 is a restriction factor and plays an antiviral role during CCHFV infection. Elevated expression of IFITM3 in platelets indicates that this could be a common mechanism by which platelets protect against viruses, including CCHFV, which may reduce platelet consumption and destruction caused by CCHFV infection. These findings provide valuable insights into the pathogenesis of CCHF-associated thrombocytopenia and offer foundational theoretical support for future therapeutic strategies.

## INTRODUCTION

Crimean-Congo hemorrhagic fever virus (CCHFV), primarily transmitted by ticks of the genus *Hyalomma*, was first identified in patients in 1956 (Akinci et al., 2013). In 1969, the causative pathogen of Crimean-Congo hemorrhagic fever (CCHF) disease in humans was found to cause disease in humans with fatality rates ranging from 10% to 50%, which was higher in some outbreaks (Fereidouni et al., 2023; Haddock et al., 2018; Aslam et al., 2023). The disease manifests with a range of severe symptoms, including fever, headache, fatigue, dizziness, gastrointestinal distress, and, more critically, hemorrhagic manifestations such as petechiae, ecchymosis, and bleeding from mucous membranes (Bodur et al., 2012; Akinci et al., 2016). A hallmark feature of CCHF is thrombocytopenia (Ergonul, 2012; Cross et al., 2020), which contributes to hemorrhagic complications. The World Health Organization has recognized CCHF as a priority infectious disease owing to its widespread

* Corresponding author.
*E-mail addresses:* shenshu@wh.iov.cn (S. Shen), df@wh.iov.cn (F. Deng)
[1] Jingyuan Zhang and Yaohui Fang contributed equally to this work.

https://doi.org/10.1016/j.virs.2025.05.002
Received 18 January 2025; Accepted 8 May 2025
Available online 21 May 2025

endemic nature, potential to cause outbreaks in new geographical regions, and the absence of specific antiviral treatments (Mcentire et al., 2021). Consequently, there is an urgent need to better elucidate virus-host interactions to advance our understanding of disease pathogenesis, which would further support the development of antiviral strategies (Bente et al., 2013).

CCHFV does not cause disease in immunocompetent adult rodents, and the only available models are neonatal mice and rats (Chumakov et al., 1968; Hoogstraal, 1979). In recent years, CCHFV infection and lethal/-severe disease models have been successfully established using IFNAR$^{-/-}$ or STAT-1$^{-/-}$ mice, which have been used to evaluate viral replication, immune responses, the efficacy of antivirals and monoclonal antibodies, and organ pathology (Tignor and Hanham, 1993; Zivcec et al., 2013; Lindquist et al., 2018; Aligholipour Farzani et al., 2019). Although CCHFV infection does not lead to fatal outcomes in immunocompetent mice, it still causes acute infection starting from the third day, as viral loads in various organs and the release of inflammatory cytokines were detected and continued to increase (Garrison et al., 2019; Tipih et al., 2023). These animal models are essential for understanding disease pathophysiology and developing potential therapeutic interventions. Because bleeding is a major feature of CCHF, it is necessary to evaluate blood-related biomarkers, including platelet counts and coagulation factors, in animal models to understand the mechanisms underlying CCHF-induced bleeding.

Platelets, key players in the coagulation cascade, also play a significant role in antiviral immune responses. Recent studies have shown that platelet function can be altered during viral infections, suggesting their contribution to host defense against pathogens (Dib et al., 2020). Dengue virus infection can induce platelet aggregation and activation, which promotes viral clearance and immune complex formation (Simon et al., 2015; Quirino-Teixeira et al., 2022). Similarly, during influenza virus infection, platelet-derived factors can enhance immune responses and viral clearance (Bote et al., 2022). Moreover, megakaryocytes, the progenitors of platelets, possess intrinsic immune recognition systems that can respond to viral infections. Recent evidence suggests that megakaryocytes can modulate antiviral immune responses through the release of pro-inflammatory cytokines and production of interferons, potentially playing a pivotal role in controlling viral replication (Campbell et al., 2019). These insights highlight the importance of platelets and megakaryocytes in the immune response to viral infections.

In this study, we characterized functional changes in platelets from CCHFV-infected experimental mice. Based on the transcriptome data, we found that interferon-induced transmembrane protein 3 (IFITM3) was significantly upregulated, suggesting its role as a key factor in protecting platelets against CCHFV infection. We evaluated IFITM3's role in suppressing CCHFV infection using a human megakaryoblast cell line with IFITM3 overexpression or knockout. The interaction between IFITM3 and the CCHFV glycoprotein, as well as the domains critical for this interaction, was further investigated. These results demonstrate an important role of platelets in the antiviral response against CCHFV infection and suggest that IFITM3 functions as a key antiviral factor by limiting viral entry through glycoprotein interactions. These findings highlight the critical role of IFITM3 in CCHFV-host interactions and antiviral activity, providing new mechanistic insights into its function.

## RESULTS

### Transcriptome of mouse platelets is altered during CCHFV infection

To investigate changes in platelets in CCHFV infection, we infected C57BL/6J mice with CCHFV. The infected C57BL/6J mice developed hemolysis and aplastic anemia (Supplementary Fig. S1). Routine blood examinations during the acute phase of infection (day 3 post-inoculation) revealed significant alterations, including decreased red blood cell count (RBC), hemoglobin (HGB), hematocrit (HCT), mean corpuscular volume (MCV), and low fluorescence reticulocyte (LFR%), and increased mean corpuscular hemoglobin concentration (MCHC), red cell distribution width-coefficient of variation (RDW-CV%), reticulocyte count (absolute) (RET#), immature reticulocyte fraction (absolute) (IRF%), and high fluorescence reticulocyte (HFR%), indicating hemolytic or regenerative anemia (Supplementary Fig. S1A). Elevated neutrophil counts and decreased lymphocyte levels suggested an acute-phase response to CCHFV infection (Supplementary Fig. S1B). Viral infection caused a marked reduction in the platelet count and an increase in platelet large cell ratio (P-LCR) and mean platelet volume (MPV), indicating platelet destruction and enhanced platelet production (Supplementary Fig. S1C). Accordingly, we observed a significant increase in plasma thrombopoietin (TPO), a glycoprotein hormone responsible for regulating platelet production and maintaining normal platelet levels (Supplementary Fig. S1D). This increase is likely associated with severe platelet depletion following CCHFV infection and subsequent acceleration of platelet production in megakaryocytes. Moreover, likely due to the early time points of sampling (3 days post-infection), we did not observe significant changes of platelet activation or coagulation in the mice with CCHFV infection, as exhibited by the reduced plasma CD62P and unchanged D-dimer levels in comparison to the control group (Supplementary Fig. S1D).

Platelets were purified from these mice and used for RNA transcriptome analysis. The results showed that the platelets from the CCHFV-infected groups formed clusters distinct from those in the control groups (Fig. 1A), suggesting a functional deviation of platelets caused by CCHFV infection compared to healthy mice. KEGG pathway analysis indicated that CCHFV infection induced functional alterations in platelets, including actin cytoskeleton regulation, platelet activation, and platelet adhesion (Fig. 1B). Additionally, platelets exhibit functional changes related to responses in other diseases, such as COVID-19 and prion disease. GO functional annotation of the differentially expressed genes (DEGs) showed significant enrichment in pathways related to protein phosphorylation, catabolism, ribonucleoprotein complex assembly, and cytoplasmic transport. These findings suggested that platelets stimulated during an antiviral response generate downstream signals that accelerate protein metabolism (Fig. 1C). A total of 1251 DEGs were identified at the nominal significance level ($P < 0.05$). Of these, 639 remained significant after stringent multiple-comparison adjustment (false discovery rate, $P < 0.05$); 372 transcripts were upregulated and 267 were downregulated. Notably, we found that the transcription of *mIfitm3* was significantly upregulated, ranking among the top 20 genes exhibiting significant differences in transcription levels compared to the control (Fig. 1D and E). Consistent with increased transcription, elevated IFITM3 expression was confirmed in the platelets of CCHFV-infected mice (Fig. 1F). These results suggest that CCHFV infection led to the loss of platelet numbers and alterations in platelet function, although platelet activation was not significant.

### Characterization of human megakaryocytes infected by CCHFV

Megakaryocytes, the progenitor cells that produce platelets, possess biological features similar to those of platelets (Machlus and Italiano, 2013; Koupenova et al., 2022). We characterized the infection and growth properties of CCHFV in the human megakaryoblast cell line MEG-01 and compared to those in HEK293 cells that express lower levels of hifitm3. Flow cytometry analysis revealed that 2.6%–2.78% of MEG-01 cells were infected with CCHFV, less than that observed in HEK293 cells (41.1%–57.3%) (Fig. 2A). The expression of CCHFV NP was detected in MEG-01 cells at 48 h post-infection (p.i.), with a slight increase thereafter. In contrast, a high level of CCHFV nucleoprotein (NP) expression was observed in HEK293 cells at 24 h p.i., and was maintained during the subsequent period examined (Fig. 2B). Additionally, we examined IFITM3 protein expression in both cell lines after CCHFV

infection. Although constitutive expression of IFITM3 was observed in MEG-01 cells, CCHFV infection resulted in increased IFITM3 expression at 24 h p.i., before CCHFV NP blotting. Unlike MEG-01, which exhibited detectable IFITM3 expression at 0 h p.i., IFITM3 was undetectable in HEK293 cells. Nevertheless, IFITM3 expression was detected at 24 h p.i. and increased thereafter (Fig. 2B). Subsequently, the increase in hifitm3 transcription in both MEG-01 and HEK293 cells after CCHFV infection was confirmed using qRT-PCR. Compared with the control group, *IFITM3* transcription increased 2.21 ± 0.62-fold in CCHFV-infected MEG-01 cells ($P < 0.05$), while HEK293 cells showed an even greater increase, peaking at 48 h p.i. with a 208.0 ± 47.92-fold elevation relative to controls ($P < 0.001$) (Fig. 2C). At 96 h p.i., the culture supernatants from MEG-01 cells

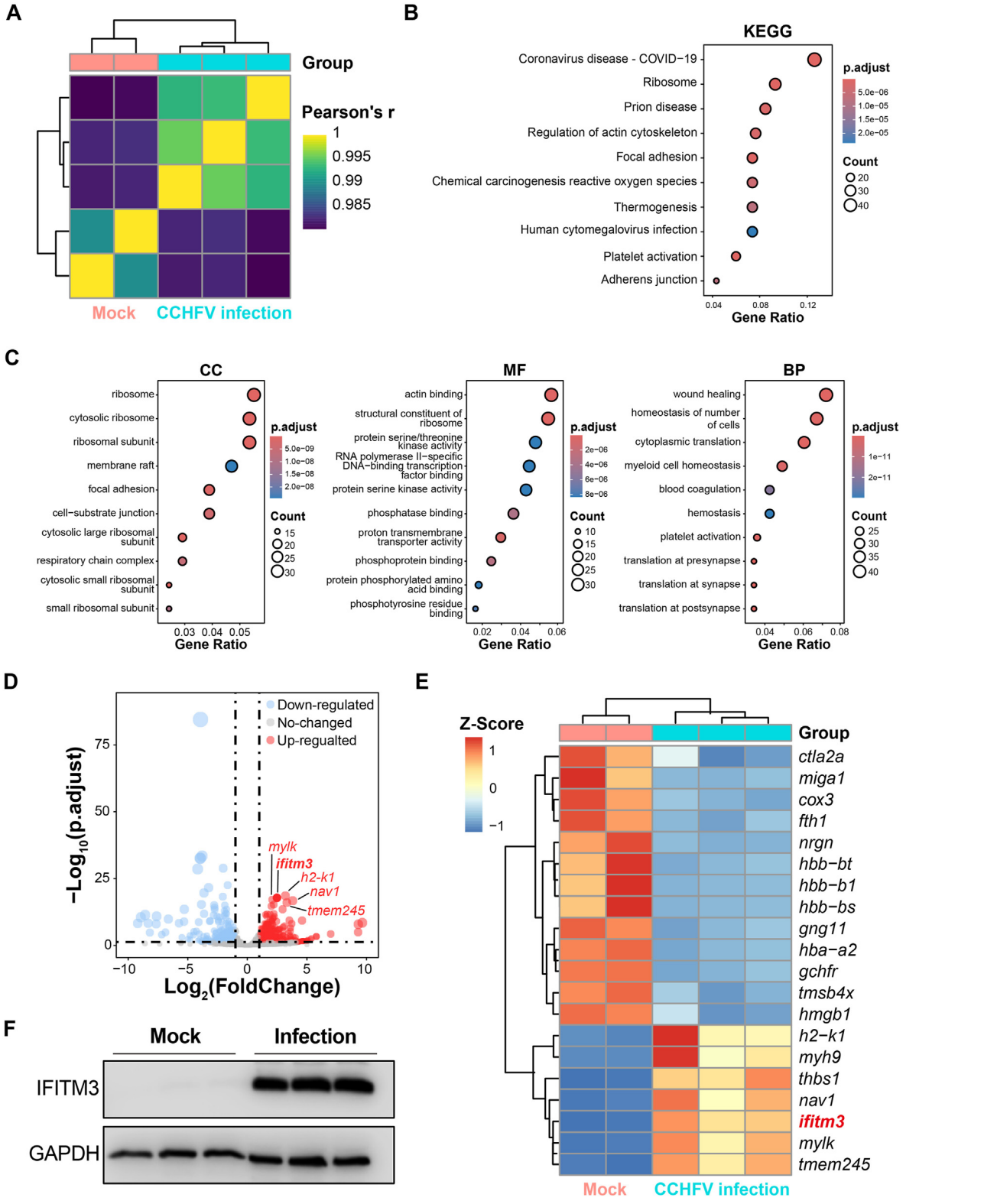


*(caption on next page)*

**Fig. 1.** Identification of differentially expressed genes in platelets of CCHFV-infected mice. Three groups of C57BL/6J mice (6–8 weeks old, female, n = 10/group) were inoculated with CCHFV ($1.56 \times 10^5$ $TCID_{50}$/mouse) intraperitoneally, and two mock groups (n = 10/group) received brain homogenate in the same route and served as control groups. On day 3 post-inoculation, mice were euthanized and blood was collected. Platelets were then purified and applied to transcriptome sequencing. **A** Hierarchical clustering of global gene expression data revealed that samples from the CCHFV-infected group (cyan) were closely clustered, and were distinct from those of the healthy group (pink). The data are presented by the Pearson correlation coefficient (Pearson's r) between different groups. **B** KEGG annotation and expression analysis of the genome. The ten pathways with the smallest adjusted *P*-values (*p.adjust*) are shown. Pathways were sorted according to gene ratio. **C** GO enrichment analysis highlighting representative functional categories enriched among differentially expressed genes (DEGs) in CCHFV-infected mice ($P < 0.01$). The ten entries with the smallest *p.adjust* from the three GO categories (CC: Cell Component; MF: Molecular Function; BP: Biological Process) are shown. **D** Volcano plot showing the differential expression of genes (DEGs) in platelets of CCHFV-infected mice in comparison to healthy controls. Red dots represent upregulated genes, blue dots indicate downregulated genes, and grey dots show genes with no significant differences. The top five genes exhibiting increased transcription levels the most significantly more than the other genes are labelled. **E** The heatmap exhibited the top 20 DEGs with a significantly increased or decreased transcription levels. The data has been normalized by row and is displayed as a z-score. **F** Validation of increased IFITM3 protein expression in platelets of infected mice via Western blot analysis, with GAPDH as the internal control. Three other groups of mice (n = 10/group) were infected with CCHFV (Infection) in the same route as described above. Platelets were purified on day 3 post-isolation. After confirming platelet purity >97%, IFITM3 expression was examined by Western blot. Platelets from three groups of healthy mice inoculated with culture medium (Mock) were used as control, and GAPDH expression was blotted as inner control of platelets.

contained $7.96 \times 10^7 \pm 2.81 \times 10^7$ copies/mL of viral RNA which was lower than that from HEK293 cells ($8.91 \times 10^8 \pm 3.99 \times 10^8$ copies/mL) at the same time point, suggesting fewer progeny viruses were produced in MEG-01 cells compared to HEK293 cells. Similarly, the viral copies in MEG-01 cells ($1.20 \times 10^6 \pm 1.32 \times 10^5$ copies/$10^3$ cells) at 96 h p.i. were also lower than those in HEK293 cells ($2.64 \times 10^6 \pm 4.01 \times 10^5$ copies/$10^3$ cells) (Fig. 2D). Accordingly, CCHFV was detected in only a limited proportion of MEG-01 cells, showing a lower infection rate compared to HEK293 cells (Fig. 2E). These results suggest that, despite being less sensitive to CCHFV than HEK293 cells, MEG-01 cells could still be infected and maintain CCHFV replication to produce progeny viruses. Furthermore, CCHFV infection upregulated IFITM3 expression in both cell lines.

## Overexpression of IFITM3 restricts infection of CCHFV

Previous studies have demonstrated that IFITM3 serves as an antiviral immune protein that suppresses various viral infections (Campbell et al., 2019; Klein et al., 2023; Du et al., 2024). Since IFITM3 was undetectable in HEK293 cells (Supplementary Fig. S2A and B), we generated an IFITM3-overexpressing cell line (HEK293-*hifitm3*-OE). Accordingly, MEG-01 cells overexpressing IFITM3 were generated (MEG-01-*hifitm3*-OE) (Supplementary Fig. S3A and B). We found that CCHFV infection was suppressed in MEG-01-*hifitm3*-OE cells, as shown by reduced CCHFV NP expression and decreased viral RNA copies in MEG-01-*hifitm3*-OE cells (Fig. 3A and B) as well as fewer cells blotted with the antibody against CCHFV NP (Fig. 3C). Similarly, IFITM3's inhibitory effect was confirmed in HEK293-*hifitm3*-OE cells (Fig. 3D–F). High levels of IFITM3 expression significantly reduced both CCHFV NP expression (Fig. 3D) and viral RNA copies in the supernatants (Fig. 3E, left). CCHFV copies also decreased at 24 h and slightly increased at 48 h. Although there was no significant difference, it suggested that IFITM3 overexpression may postpone the intracellular replication of CCHFV in HEK293 cells (Fig. 3E, right). As expected, CCHFV infection was immunostained in very few HEK293-*hifitm3*-OE cells (Fig. 3F). These results demonstrate that IFITM3 exerts a strong inhibitory effect on CCHFV infection in both MEG-01 and HEK293 cells.

## Knockout of IFITM3 promotes infection of CCHFV

Subsequently, together with MEG-01, the HeLa cell line was selected to generate IFITM3-knockout cells, as HeLa exhibited a higher expression of IFITM3 than MEG-01 cells (Supplementary Fig. S2A and B), resulting in MEG-01-*hifitm3*-KO and HeLa-*hifitm3*-KO cells, respectively (Supplementary Fig. S3C and D), In either MEG-01-*hifitm3*-KO cells or HeLa-*hifitm3*-KO cells, the knockout of *hifitm3* led to enhanced infection with CCHFV. We detected increased CCHFV NP expression (Fig. 4A and D), elevated CCHFV RNA copies in cells and supernatants (Fig. 4B and E), and enhanced immunostaining of cells with the CCHFV NP antibody (Fig. 4C and F). These results demonstrate that in the absence of IFITM3, CCHFV infection is enhanced, further supporting that IFITM3 presents an inhibitory effect on CCHFV infection.

## IFITM3 suppresses CCHFV entry into cells via interacting with CCHFV Gc

We hypothesized that human IFITM3 might interact with CCHFV proteins. Since MEG-01 cells exist in a semi-adherent/semi-suspended state in the culture supernatant, resulting in cell loss during transfection experiment, both MEG-01 and HEK293 cell lines exhibit limited IFITM3 baseline expression, and overexpression of IFITM3 showed an inhibitory effect on CCHFV infection. Therefore, we performed pull-down assays using lysates from HEK293 cells transfected with an IFITM3-expressing plasmid and infected with CCHFV. CCHFV Gc specifically precipitated with IFITM3, suggesting an interaction between IFITM3 and CCHFV Gc other than with Gn and NP (Fig. 5A). Additionally, the co-localization of IFITM3 and Gc was observed in the cytoplasm of HEK293 cells infected with CCHFV (Fig. 5B). We subsequently analyzed the effects of IFITM3 on CCHFV entry into host cells. Overexpression of IFITM3 in MEG-01 cells significantly reduced the amount of virus bound to the cell surface and internalized into the cells (Fig. 5C).

## CIL-TMD domain is critical for the interaction between IFITM3 and Gc

Subsequently, the interaction between IFITM3 and CCHFV Gc was confirmed by pull-down analysis using lysates from HEK293T cells co-transfected with plasmids expressing both proteins (Fig. 6A). The truncated IFITM3 constructs were generated according to a previous study (Xu et al., 2022), including NTD, IMD-CIL, and CIL-TMD, which were fused with EGFP (Fig. 6B). Moreover, the co-localization of IFITM3 and CCHFV Gc was observed in co-transfected cells (Fig. 6C). Pull-down analyses were performed using cells co-transfected with plasmids expressing IFITM3 truncates and CCHFV Gc. The results showed that both IMD-CIL and CIL-TMD could precipitate CCHFV Gc, with higher efficiency for CIL-TMD than for IMD-CIL (Fig. 6D). Moreover, similar to full-length IFITM3, CIL-TMD co-localized with CCHFV Gc in the cytoplasm (Fig. 6E). Computational modeling using AlphaFold 3 and PDBePISA v1.52 predicted an interaction complex where IFITM3 binds CCHFV Gc primarily through hydrogen bonds involving key residues in the CIL (Asp92), TMD (Cys105), and CTD (Tyr132) domains (Fig. 6F; Supplementary Table S1).

## DISCUSSION

CCHF, caused by CCHFV infection, is a tick-borne viral hemorrhagic fever with high human fatality rates (Mo et al., 2023). However, few studies have focused on the mechanisms underlying coagulation

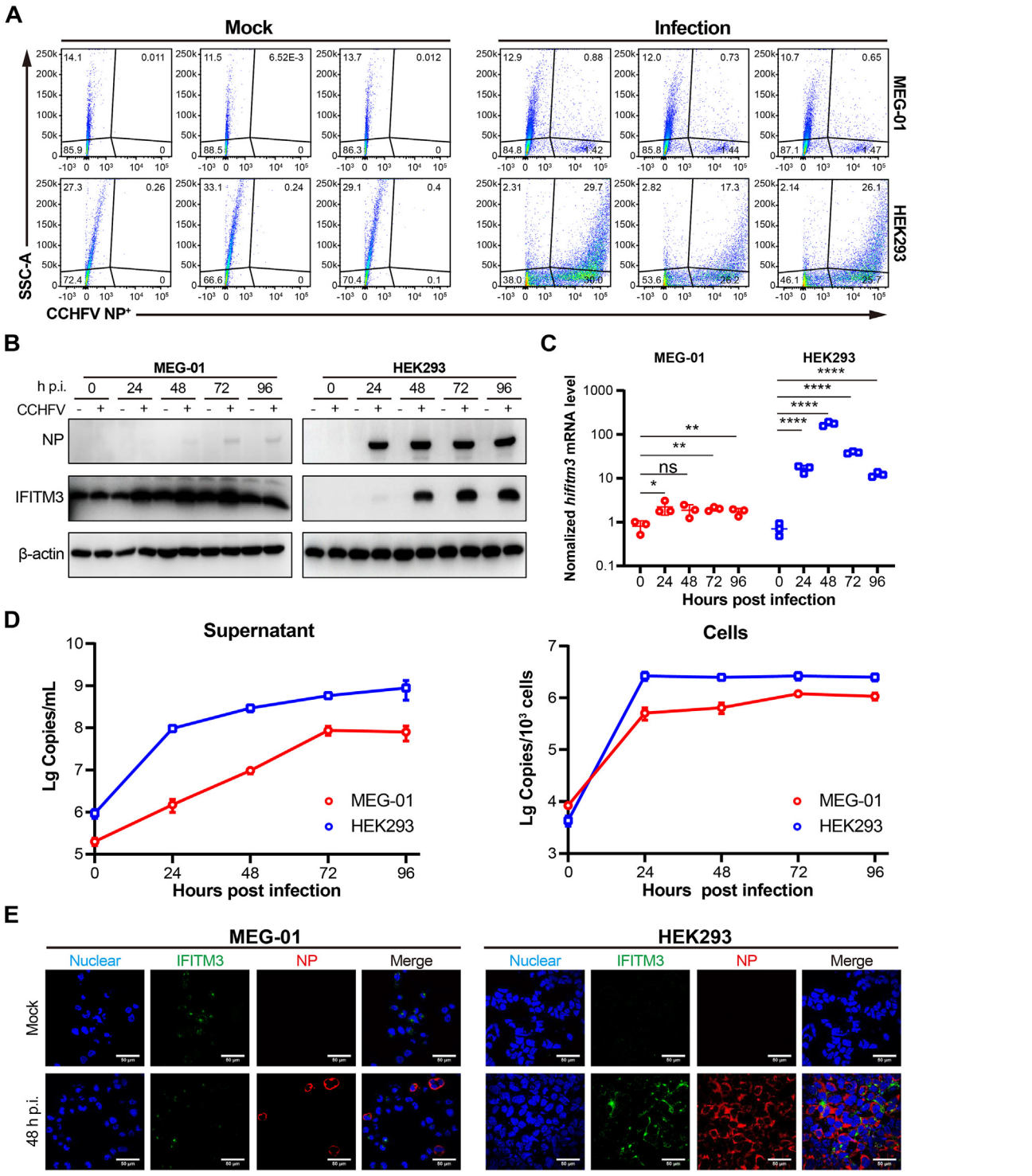


**Fig. 2.** Characterization of the properties of CCHFV infection in MEG-01 and HEK293 Cells. MEG-01 and HEK293 cells seeded in 24-well plates were incubated with CCHFV (MOI = 5) for 2 h. After infection, cells were washed three times with PBS and cultured at 37 °C in a 5% $CO_2$ incubator. Cells were collected at indicated time points for subsequent analyses. **A** The CCHFV infection efficiencies in MEG-01 and HEK293 cells collected at 48 h p.i. were analyzed by flow cytometry using CCHFV NP antibody. **B** CCHFV NP and IFITM3 expression were examined by Western blotting in MEG-01 and HEK293 cells collected at indicated time points post CCHFV infection, with β-actin as the inner control. **C** The transcription levels of *ifitm3* in MEG-01 and HEK293 cells were examined by qRT-PCR at indicated time points post CCHFV infection, and were normalized to GAPDH. **D** Quantitative analysis of the viral copies by qRT-PCR in the culture supernatant (left) and in the MEG-01 and HEK293 cells (right), respectively. **E** Visualization of CCHFV infection in MEG-01 and HEK293 cells by IFAs. IFITM3 and CCHFV NP expression was blotted in cells infected with CCHFV at 48 h p.i. or with mock infection. Cells were immunostained using antibodies against CCHFV NP (red) and IFITM3 (green), respectively. Nuclei were stained with Hoechst33258 (blue). Scale bar, 50 μm. Differences between the two groups were analyzed using One-way ANOVA to calculate the *P*-value to evaluate the differences in expression levels at different time points in the same group. $P < 0.05$ was considered statistically significant.

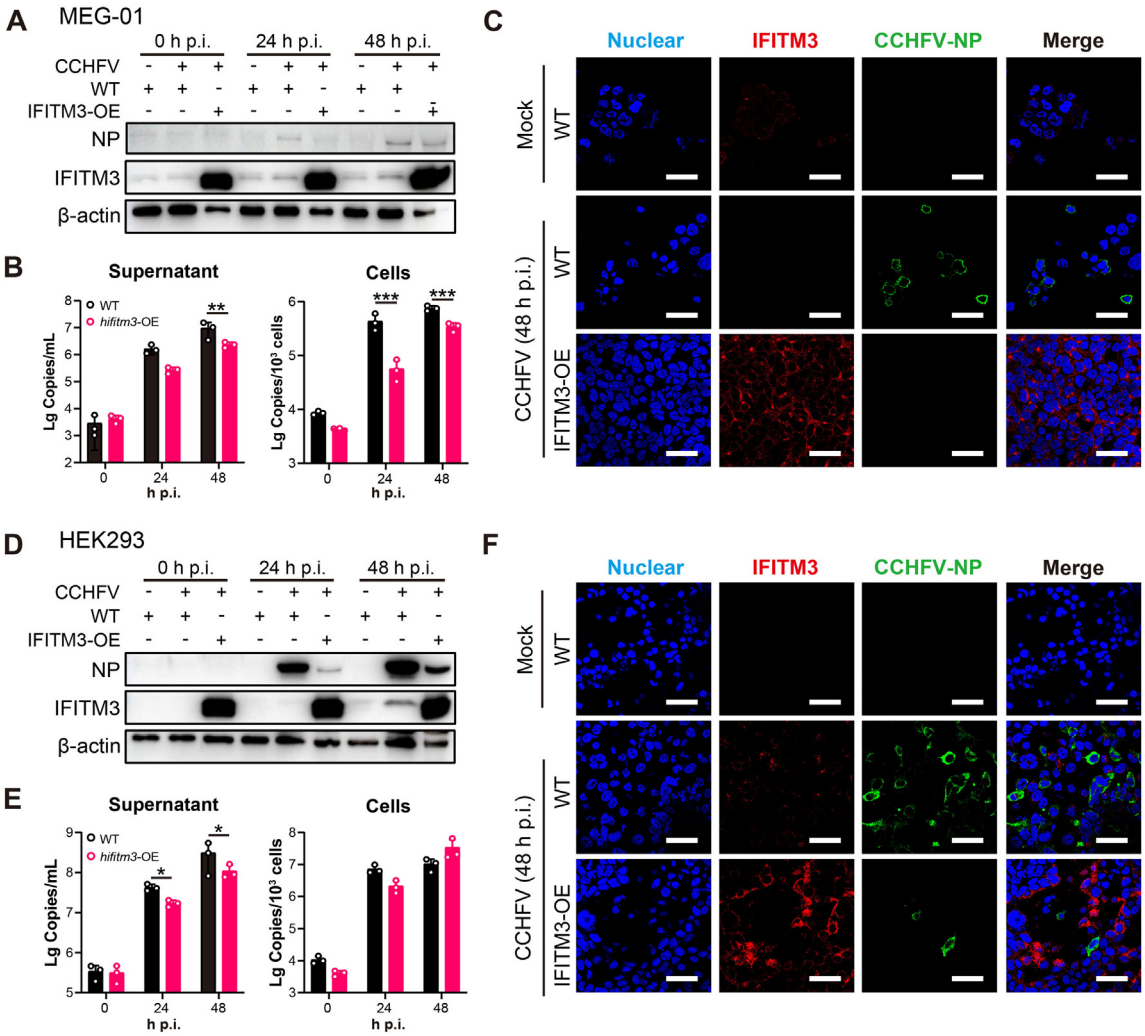


**Fig. 3.** Overexpression of IFITM3 inhibits CCHFV infection in MEG-01 **(A–C)** and HEK293 **(D–F)** Cells. Cells were infected with CCHFV (MOI=5) and collected at indicated time points for subsequent analyses. **A** Western blot analyses of CCHFV NP and IFITM3 expression in MEG-01 (WT) and MEG-01-*hifitm3*-OE (IFITM3-OE) cells at indicated time points, with β-actin as the internal control. **B** Quantitative RT-PCR to determine the RNA loads of CCHFV S segment in both supernatants (left) and cells (right) at indicated time points. **C** Confocal microscopy images showing CCHFV NP and IFITM3 expression and subcellular localization. Cells are immunostained using antibodies against CCHFV NP (green) and IFITM3 (red), respectively. **D** Western blot analyses of CCHFV NP and IFITM3 expression in HEK293 (WT) and HEK293-*hifitm3*-OE (IFITM3-OE) cells at indicated time points, with β-actin as the internal control. **E** Quantitative RT-PCR to determine the RNA loads of CCHFV S segment in both supernatants (left) and cells (right) at indicated time points. **F** Confocal microscopy images showing CCHFV NP and IFITM3 expression and subcellular localization. Cells were immunostained using antibodies against CCHFV NP (green) and IFITM3 (red), respectively. Nuclei were stained with Hoechst33258 (blue). Images were taken using a Leica confocal microscope. Scale bar, 20 μm. The data between groups were analyzed using two-way ANOVA. Data are expressed as the mean ± SD. $P < 0.05$ indicates a statistically significant difference, $^{*}P < 0.05$, $^{**}P < 0.01$, $^{****}P < 0.0001$.

disorders caused by CCHFV infection. In the present study, we found that CCHFV-infected C57BL/6J mice did not exhibit any obvious clinical symptoms. However, they may develop hemolysis and aplastic anemia despite not showing significant platelet activation or coagulopathy. Platelets function in hemostasis and mediate immune responses. We subsequently characterized functional changes in platelets purified from infected mice using RNA transcriptome analysis. Functional alterations in platelets were mainly involved in platelet activation, adhesion, and regulation of the actin cytoskeleton. Significant changes were observed in the pathways associated with protein phosphorylation, catabolism, ribonucleoprotein complex assembly, and cytoplasmic transport. This demonstrates the important role of platelets in responding to CCHFV infection, probably more so than in hemostasis. Similarly, functional alterations were observed in platelets from mice with infection SFTSV (Fang et al., 2024). Despite the different functional changes based on transcriptomic analyses, coagulation, platelet activation, and immune modulation found in platelets of SFTSV-infected mice were also identified in platelets of CCHFV-infected mice in the current study. This may suggest a common response by platelets to tick-borne virus infections, while virus-specific responses are also worth considering.

IFITM3, an interferon-induced membrane protein, is considered an antiviral factor that inhibits viral entry and replication (Bailey et al., 2013, 2014) such as HCV (Yao et al., 2011; Narayana et al., 2015), HIV (Lu et al., 2011; Tartour et al., 2014; Compton et al., 2016), and influenza (Bailey et al., 2013; Ren et al., 2020). Our study revealed the significant increase of IFITM3 expression in platelets of CCHFV-infected mice, which was also supported by the previous study reporting the significant upregulation of IFITM3 in PBMCs of patients with CCHF, dengue, and influenza (Campbell et al., 2019; Neogi et al., 2022; Denz et al., 2024). This suggests that increased IFITM3 in platelets may play an important role in the antiviral responses commonly observed in viral diseases. Due

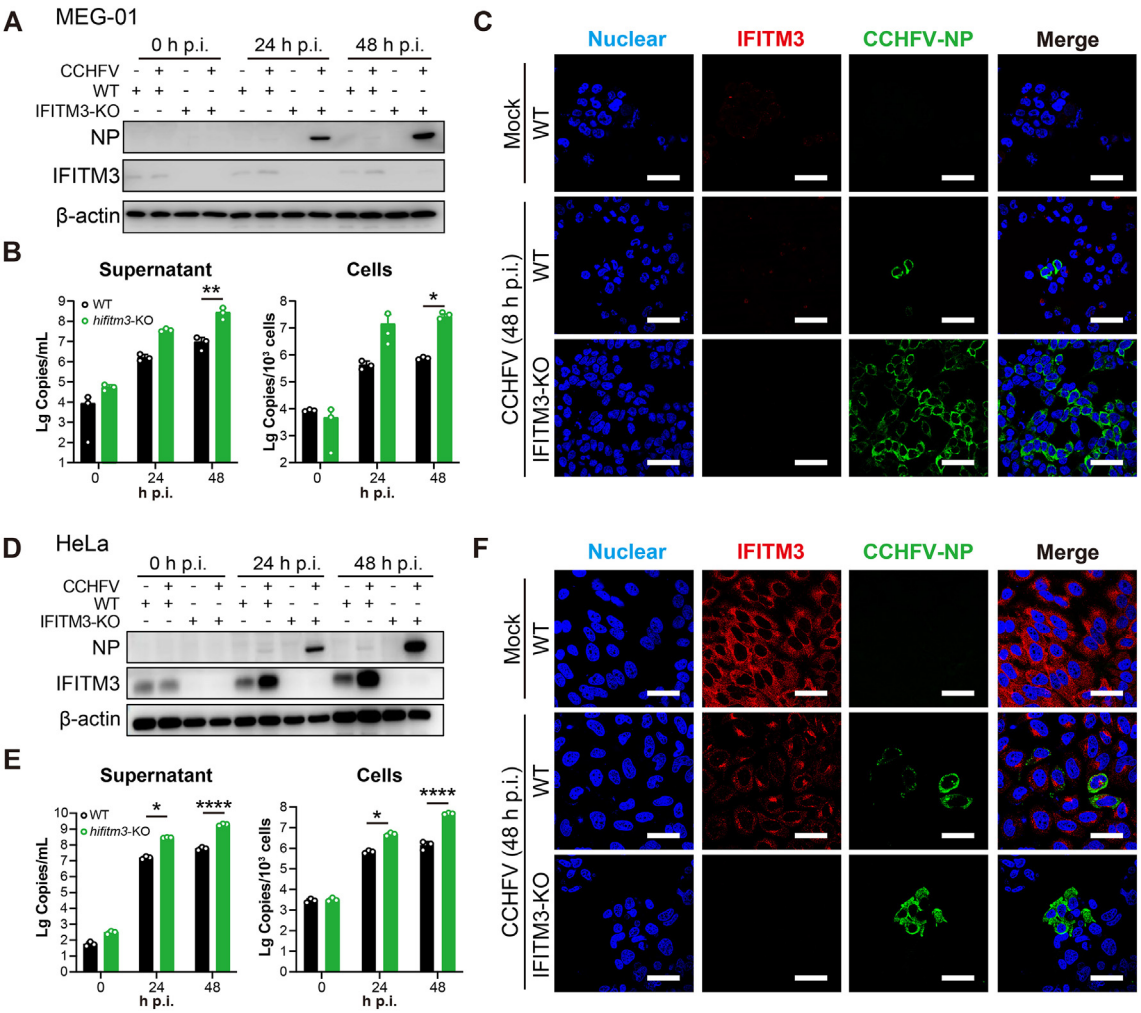


**Fig. 4.** Knockout IFITM3 promotes CCHFV infection in MEG-01 **(A–C)** and HeLa **(D–F)** cells. Cells were infected with CCHFV (MOI = 5), and collected at indicated time points for subsequent analyses. **A** Western blot analyses of CCHFV NP and IFITM3 expression in MEG-01 (WT) and MEG-01-*hifitm3*-KO (IFITM3-KO) cells at indicated time points, with β-actin as the internal control. **B** Quantitative RT-PCR to determine the RNA loads of CCHFV S segment in both supernatants (left) and cells (right) at indicated time points. **C** Confocal microscopy images showing CCHFV NP and IFITM3 expression and subcellular localization. Cells are immunostained using antibodies against CCHFV NP (green) and IFITM3 (red), respectively. **D** Western blot analyses of CCHFV NP and IFITM3 expression in HeLa (WT) and HeLa-*hifitm3*-KO (IFITM3-KO) cells at indicated time points, with β-actin as the internal control. **E** Quantitative RT-PCR to determine the RNA loads of CCHFV S segment in both supernatants (left) and cells (right) at indicated time points. **F** Confocal microscopy images showing CCHFV NP and IFITM3 expression and subcellular localization. Cells were immunostained using antibodies against CCHFV NP (green) and IFITM3 (red), respectively, and nuclei were stained with Hoechst33258 (blue). Images were taken using a Leica confocal microscope. Scale bar, 20 μm. The data between groups were analyzed using two-way ANOVA. Data are expressed as the mean ± SD. $P < 0.05$ indicates a statistically significant difference, $^{*}P < 0.05$, $^{**}P < 0.01$, $^{****}P < 0.0001$.

to the limited ability to manipulate IFITM3 expression in platelets, we subsequently generated IFITM3 overexpressing and knockout cell lines using the human megakaryoblast cell line MEG-01. We characterized the effects of CCHFV infection on megakaryocytes and evaluated the role of IFITM3 in CCHFV infection using these generated cell lines, comparing them with other cell lines containing high (HeLa) or undetectable (HEK293) levels of IFITM3. Despite the less efficient infection of CCHFV in MEG-01 cells than that in HEK293 cells, MEG-01 cells maintained CCHFV proliferation to generate progeny viruses. CCHFV infection increased IFITM3 expression in both MEG-01 and HEK293 cells. This result contradicts the inhibitory effect of IFITM3 on CCHFV infection observed in MEG-01-*hifitm3*-OE and HEK293-*hifitm3*-OE cells infected with CCHFV. IFITM3 exerts its inhibitory effect by affecting the virus-host cell membrane fusion process and restricts the infection of various enveloped viruses during the early stages of viral entry (Zani and Yount, 2018). The generated cell lines, MEG-01-*hifitm3*-OE and HEK293-*hifitm3*-OE, already exhibited the overexpressed IFITM3, which inhibits CCHFV infection by suppressing its entry process. However, in HEK293 cells, IFITM3 expression was induced by CCHFV infection, and its expression was detected immediately after CCHFV NP was detected. Increased IFITM3 had a very limited effect on the inhibition of CCHFV infection. Because MEG-01 cells naturally express a certain level of IFITM3, CCHFV infection may be inhibited. As a result, the efficiency of CCHFV infection in MEG-01 cells is relatively low. Moreover, the inhibitory effect of IFITM3 on CCHFV infection was further confirmed in IFITM3-knockout MEG-01 and HeLa cells, as infection was significantly enhanced. CCHFV exhibited varied infection efficiencies, which can be attributed to the differing sensitivities of various cell lines of distinct tissue origins (Dai et al., 2021). So, the levels of IFN response stimulated by CCHFV infection may also vary, thus affecting the expression levels of IFITM3 (Scholte et al., 2017). Therefore, the inhibitory effect of IFITM3 on CCHFV infection may also depend on the infection efficiency of CCHFV in different cell lines.

Subsequently, the interaction between IFITM3 and CCHFV Gc was identified, which resulted in reduced efficiency of viral binding and internalization of CCHFV into MEG-01 cells. We postulated that the

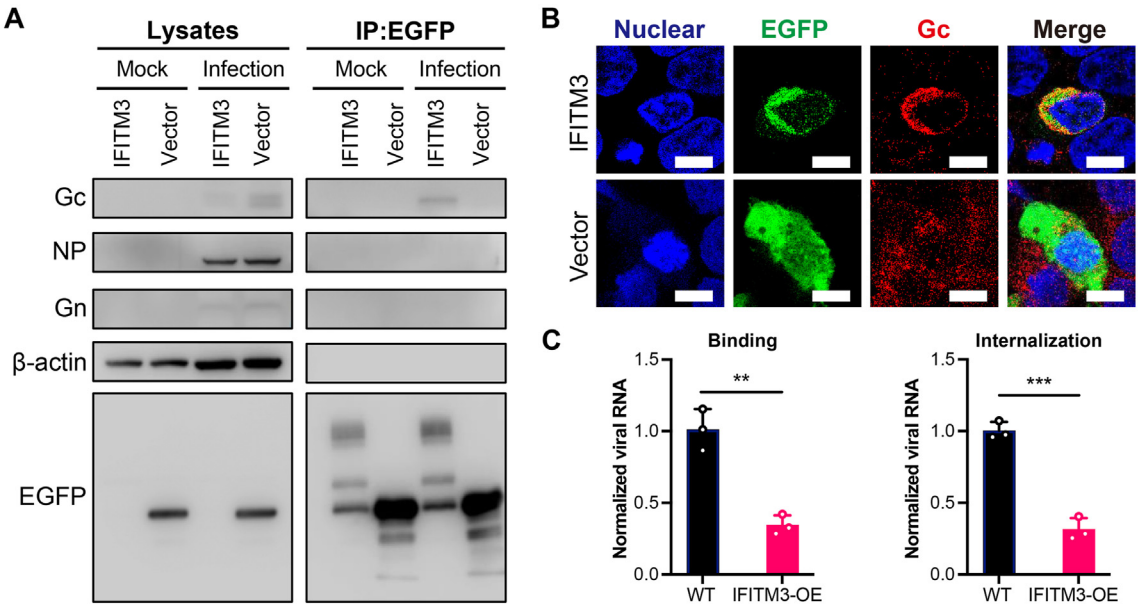


**Fig. 5.** IFITM3 interacts with CCHFV Gc protein. HEK293T cells were transfected with pEGFP-N1-*hifitm3* (IFITM3) or pEGFP-N1 (Vector) for 24 h and then infected with CCHFV (MOI = 5) for 48 h. After lysis, the cells were pulled down with the beads against the enhanced green fluorescent protein (anti-EGFP). **A** Western blot analyses of CCHFV Gc, NP, and Gn, EGFP, and β-actin in the cell lysates and outputs after pulling down using anti-EGFP. **B** Confocal microscopy images showing the viral protein (Gc) and IFITM3 (EGFP) are co-localized. Images were taken using a Leica confocal microscope. Scale bar, 20 μm. **C** Quantification of CCHFV (MOI = 10) binding (left) and internalization (right) to MEG-01 (WT) and MEG-01-*hifitm3*-OE (IFITM3-OE) cells. For binding assays, cells were incubated with CCHFV on ice for 1 h and were washed three times with ice-cold PBS to remove unbound viruses. Cells were then harvested to determine CCHFV S RNA by qRT-PCR. For internalization assays, cells were incubated with CCHFV at 4 °C for 1 h, then moved to 37 °C and incubated for 1h to allow viral internalization. Cells were washed with PBS containing 500 ng/mL proteinase K to remove the uninternalized virus. Internalized viruses were quantified by qRT-PCR. GAPDH was blotted as an internal control. The CCHFV RNA loads were normalized to MEG-01 cells using $2^{-\Delta\Delta Ct}$ method. The significant difference was determined using the student's *t-test*. $P < 0.05$ indicates a statistically significant difference, $^{**}P < 0.01$, $^{***}P < 0.001$.

interaction between IFITM3 and CCHFV Gc suppresses the fusion process. However, because of the limited infection rates in MEG-01 cells, we were unable to characterize the effect of IFITM3 on syncytia formation. Nevertheless, our results demonstrate that IFITM3 plays a role in suppressing CCHFV entry, which is consistent with a previous study reporting that IFITM3 inhibits viral entry by interacting with SFTSV Gc (Denz et al., 2024; Du et al., 2024). CCHFV is a genetically diverse virus that is currently divided into seven major genotypes (I-VII), each with significant association with their geographical distributions (Deyde et al., 2006; Bente et al., 2013). It is possible that different strains or genotypes of CCHFV could affect the interaction with IFITM3, as there may be amino acid substitutions at key positions. Further studies are needed to characterize roles of key sites in the interaction between IFITM3 and CCHFV Gc. Furthermore, we found that IFITM3 interacts with CCHFV Gc and that the CIL-TMD region of IFITM3 is critical for this interaction. CCHFV enters cells via clathrin-mediated endocytosis. It can interact with inner membrane proteins in early endosomes, through which CCHFV RNA is released into host cells (Shtanko et al., 2014). IFITM3 is located on the endosomal membrane. Although the spatial topological structure of IFITM3 remains unclear, the CIL domain has been suggested to be located on the inner side of the endosome (Marziali et al., 2021). We speculated that elevated IFITM3 expression increases the possibility that CIL interacts with Gc during CCHFV entry. As a result, CCHFV internalization is suppressed, which reduces the infection rate of this virus.

IFITM3 is a downstream gene induced by interferon signaling. The expression level of IFITM3 depends on the activation levels of IFN signaling (Schoggins et al., 2011). Following viral infection, the interferon signaling pathway upregulates IFITM3 expression, further inhibiting viral replication, and potentially constituting a broad-spectrum antiviral mechanism in various cell types including platelets and megakaryocytes. IFITM3 has a dynamic bidirectional regulatory ability on the IFN signaling pathway. While it enhances the early antiviral response by promoting pattern recognition receptor (PRR) signaling and stabilizing signal transducer and activator of transcription 1 (STAT1) (Jia et al., 2012; Zhang, P. et al., 2024), it can conversely prevent immunopathological damage caused by excessive production of IFN-I by blocking MAVS aggregation and upregulating SOCS (Chen et al., 2017; Lin et al., 2020), making IFITM3 a key molecule for balancing antiviral efficacy and immune homeostasis. Thus, IFITM3 has been considered a target for the treatment of infection and autoimmune diseases (Li et al., 2025). In viral hemorrhagic fever viral diseases, such as CCHF, patients would develop severe thrombocytopenia, manifested by a significant decrease in platelet count (Akinci et al., 2013; Bente et al., 2013). Although the antiviral function of IFITM3 is not entirely dependent on the interferon pathway, it can enhance the overall antiviral state by maintaining ISG expression. Its direct regulatory effect on the interferon pathway is limited and cell type specific. The expression level of IFITM3 may significantly affect the balance of the IFN signaling pathway, thereby changing the homeostasis between antiviral immune efficacy and immunopathological damage (Brass et al., 2009; Dai et al., 2021), which may be attributed to the extensive damage or consumption of platelets caused by viral infection. The elevated expression of IFITM3 in platelets demonstrates potent inhibitory effects against CCHFV infection. However, the mechanistic basis of this antiviral activity, particularly whether IFITM3 modulates platelet-mediated immune regulation through type I interferon pathway potentiation to enhance antiviral functions, requires further elucidation.

This study has several limitations. While we performed platelet transcriptome analyses using infected mouse models, these may not completely reflect platelet responses in human patients. Nevertheless, the upregulation of IFITM3 observed in our transcriptome data has been reported in platelet transcriptomes across various diseases, suggesting its role in a common antiviral mechanism. No cases of CCHFV infection have been reported in China since 2005. Without clinical samples, we could not investigate the platelet responses induced by CCHFV infection, including coagulation disorders and immune-mediated responses. It

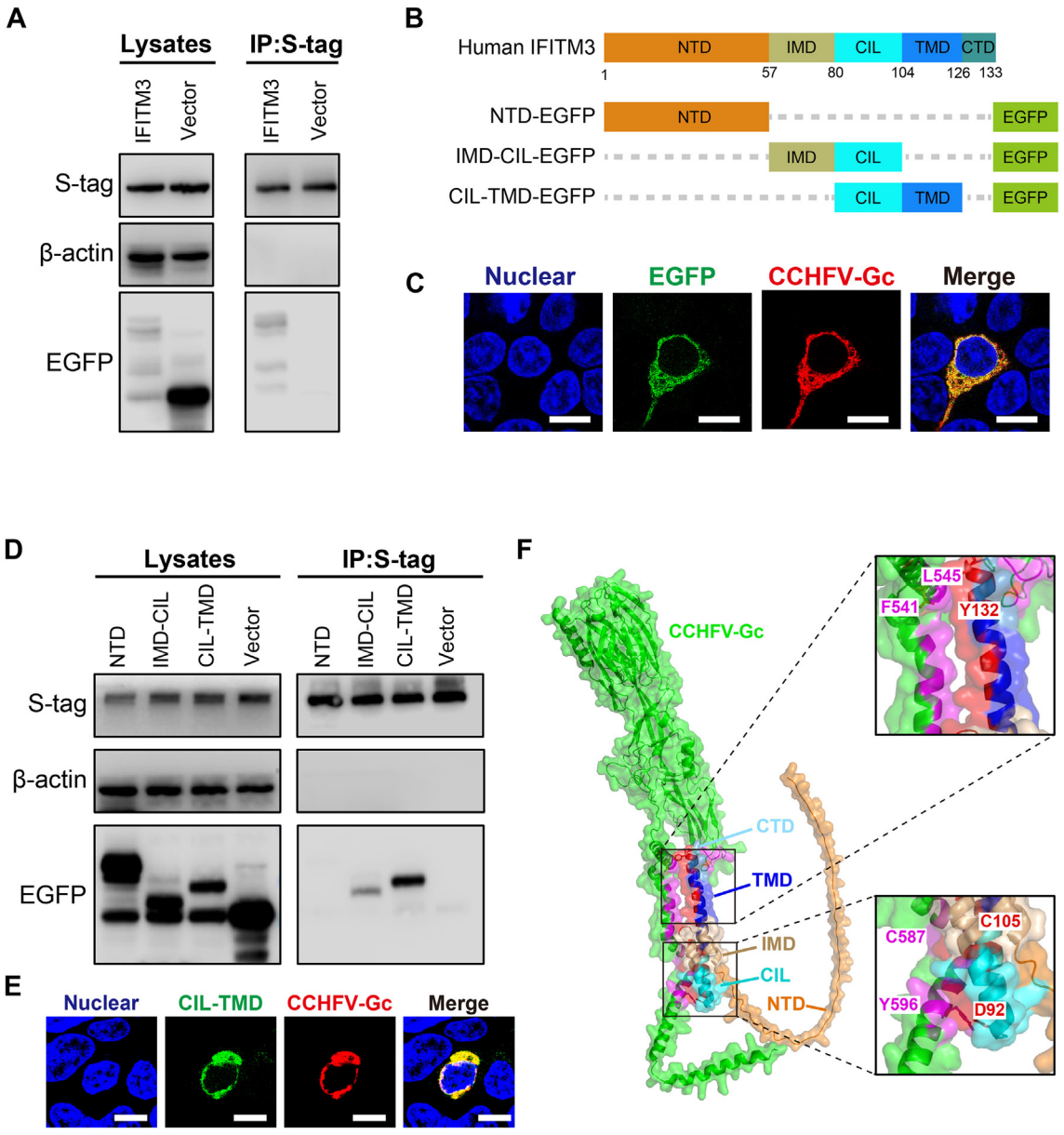


**Fig. 6.** CIL-TMD binds to the CCHFV Gc. HEK293T cells were co-transfected with phMCV-Gc-S-tag together with the pEGFP-N1 plasmid expressing IFITM3 or the truncated IFITM3 fragments or the pEGFP-N1 plasmid as control (Vector). At 24 h post transfection, cells were collected and lysed using an IP buffer. **A and D** The interaction of IFITM3 and its truncated fragments with CCHFV Gc were analyzed via S-pulldown assays followed by Western blotting, with β-actin as the internal control. **B** Schematic diagram of the constructs of truncated IFITM3 used in this study, each fused with EGFP at its N terminus. **C and E** Visualization of IFITM3 or its truncations (green) and CCHFV Gc (red) in cells using confocal microscopy. The transfected cells were fixed and permeabilized, and then incubated with S-tag antibody by IFAs. Nuclei were stained with Hoechst 33,258. Scale bar, 10 μm. **F** Schematic diagram of the 3D structures of IFITM3 and CCHFV Gc, which were predicted using Alpha fold 3. The IFITM3 domains and the regions and amino acids which could be involved in the interaction are indicated.

would be valuable to compare these data with data from CCHFV-infected animal models and actual clinical cases to elucidate commonalities and differences if relevant public datasets become available. Despite these limitations, our findings shed light on the pathogenic mechanisms of CCHF and facilitate the development of antiviral strategies.

## CONCLUSIONS

This study reveals platelet functional alterations during CCHFV infection through transcriptomic analysis. We identified IFITM3 as one of the most significantly upregulated genes in platelets of mice with CCHFV infection and demonstrated its antiviral role in suppressing CCHFV infection using MEG-01 cells. Furthermore, the interaction of IFITM3 with the CCHFV Gc protein was identified, and the CIL-TMD domain played a key role in this interaction. The findings suggest that platelets play an important role in the antiviral response to suppress CCHFV infection via elevation of IFITM3, which may facilitate future research on the pathogenesis of CCHFV-induced thrombocytopenia.

## MATERIALS AND METHODS

### Virus, cells, and antibodies

The CCHFV strain YL16070 (GenBank accession: KY354082) (Guo et al., 2017; Dai et al., 2021) used in this study was deposited at the National Virus Resource Center (IVCAS 6.6329). Titers were determined using the

endpoint dilution method as described previously (Dai et al., 2021). All experiments involving CCHFV were performed in a biosafety level 3 laboratory at the Wuhan Institute of Virology, Chinese Academy of Sciences.

Human megakaryoblast MEG-01 cells (CRL-2021, ATCC) were maintained in RPMI 1640 medium. Human embryonic kidney HEK293 (CRL-1573, ATCC), human cervical adenocarcinoma HeLa (CCL-2, ATCC) cells, and African green monkey kidney clone E6 (Vero E6) cells were maintained in Eagle's Minimum Essential Medium (EMEM, New Zongke Biotech, Wuhan, China) and human embryonic kidney HEK293T (CRL-3216, ATCC) were maintained in Dulbecco's Modified Eagle's Medium (DMEM, New Zongke Biotech, Wuhan, China) at 37 °C with 5% $CO_2$. All culture media were supplemented with 10% fetal bovine serum (FBS) and 1% penicillin-streptomycin-glutamine (Thermo Fisher Scientific, Waltham, MA, USA).

PE/Cy7® Anti-mouse CD41 Antibody [MWReg30] (ab95726), Goat Anti-Rabbit IgG H&L (Alexa Fluor® 488, ab150077), and Goat Anti-Rabbit IgG H&L (Alexa Fluor® 555, ab150078) were purchased from Abcam (Cambridge, UK). Polyclonal antibodies against the nucleoprotein (anti-NP) and N- and C-terminal fragments of the glycoproteins (Gn and Gc) of the CCHFV were prepared as previously described (Dai et al., 2021). Horseradish peroxidase (HRP)-conjugated Affinipure goat Anti-mouse IgG (H + L) (SA00001-1) and HRP-conjugated Affinipure Goat Anti-Rabbit IgG (H + L) (SA00001-2) were purchased from Proteintech Group, Inc (Chicago, IL, USA). The rabbit anti-human IFITM3 antibody ([KO Validated] IFITM3 Rabbit pAb (A13070)), which is capable to recognize both human and mouse IFITM3, was purchased from ABclonal Technology, Inc (Wuhan, China).

## Mouse experiments

A total of 120 SPF-grade C57BL/6J mice (female, 6–8 weeks) were procured from the Animal Experiment Center of the Wuhan Institute of Virology, Chinese Academy of Sciences. Mice were intraperitoneally inoculated with 200 μL of CCHFV (n = 65, $1.56 \times 10^5$ $TCID_{50}$/mouse) or received mock infection of mouse brain homogenate prepared in equivalent volume of serum-free EMEM (n = 55, 200 μL/mouse) as control. On day three post-inoculation, whole blood was collected. Platelets were purified from three groups with CCHFV infection and two groups with mock infection (n = 10/group) and were applied to transcriptome analyses. For Western blot analyses, platelets were purified from three mouse groups with CCHFV infection and three mock-infected groups (n = 10/group). Routine blood examination was carried out using blood from five mice with CCHFV infection and five others with mock infection, respectively. All animal experiments were approved by the Ethics Committee of the Wuhan Institute of Virology, Chinese Academy of Sciences (approval number: WIVA33202107) and conducted in an ABSL-3 (Animal Biosafety Level 3) laboratory.

## Platelet isolation from mice

Platelets were isolated from C57BL/6J mice and quantified by RNA sequencing. Briefly, blood collected in a vessel containing sodium citrate (w/v, 3.8%) was centrifuged at 200 ×*g* for 20 min at 25 °C to separate platelet-rich plasma (PRP) from the blood cells. The PRP was transferred to a new tube, centrifuged (200 ×*g*, 10 min) to remove residual leukocytes and red blood cells, and centrifuged at 500 ×*g* for 5 min to obtain platelet pellets. Platelets were washed with PIPES buffer (145 mM NaCl, 4 mM KCl, 50 mM $Na_2HPO_4$, 1 mM $MgCl_2{\cdot}6H_2O$, 5 mM PIPES, 5.5 mM glucose, and 300 nM prostaglandin E1) and re-suspended in serum-free M199 medium (Gibco®, Thermo Fisher Scientific, Waltham, MA, USA). Platelet purity ($CD41^+ > 97\%$) was measured using flow cytometry after incubation with PE/Cy7® anti-mouse CD41 Antibody [MWReg30].

## RNA data analysis

Total RNA was purified from platelets with or without CCHFV infection using TRIzol reagent (NovaStar, China), following the manufacturer's instructions. RNA-seq libraries were constructed according to the standard process for mRNA sequencing at the Beijing Genomics Institute (BGI, China). Raw data were filtered using SOAPnuke software (v.1.5.2). Gene expression levels were quantified in salmon (v.1.10.3) using Mus musculus GRCm39 as an index. The differential gene expression and KEGG pathway enrichment analyses were performed using DESeq2 (version 1.38.3) and ClusterProfiler (version 4.6.2), respectively. DEGs were selected using $padj < 0.05$, $\log_2$FoldChange >1, and enrichment pathways were selected based on a $P < 0.05$. Graphs and analyses of the data were generated using R (v.4.2.3) and ggplot2 (v.3.4.2) with custom scripts.

## Virus infection assay

HEK293 cells or MEG-01 cells ($1 \times 10^5$ cells per well) were infected with CCHFV (MOI = 10) at 37 °C and 5% $CO_2$ for 2 h. The cells were washed three times with phosphate-buffered saline (PBS) to remove any remaining free virus and maintained in fresh medium. Cells were collected at the indicated time points and subjected to Western blotting, qRT-PCR, and flow cytometry to determine the CCHFV infection levels.

## Western blots

After viral infection, the cells were washed with PBS (pH 7.4) and lysed in RIPA buffer containing protease inhibitors. Proteins were boiled at 100 °C for 10 min, then centrifuged for 10 min, and subjected to 12% sodium dodecyl sulfate-polyacrylamide gel electrophoresis and transferred into polyvinylidene fluoride (PVDF) membranes (Whatman, England). Membranes were blocked in Tris-buffered saline (TBS) supplemented with 0.1% Tween 20 plus 5% non-fat milk for 1 h before incubation overnight with primary antibodies at 4 °C. After washing five times, membranes were revealed using peroxidase-conjugated corresponding secondary antibodies for 1 h at 37 °C. Band signals were detected using chemiluminescence (Azure Biosystems, USA) with Super Signal West Pico Chemiluminescent Substrate (Thermo Scientific, USA), according to the manufacturer's protocol.

## Flow cytometry assay

Cells were harvested by centrifugation at 500 ×*g* for 5 min, and the pellets were washed with cold PBS, fixed with 4% paraformaldehyde for 10 min, centrifuged at 500 ×*g* for 5 min to remove paraformaldehyde, and washed with PBS again. Thereafter, the cells were stained with primary antibodies at 4 °C overnight. After washing, cells were incubated with appropriate secondary antibodies in the dark and then subjected to flow cytometric analysis using a flow cytometer (BD Biosciences, USA). Each experiment was performed in triplicates and repeated at least three times. The data generated by flow cytometry were statistically analyzed using FlowJo V10 software.

## Immunofluorescence and confocal microscopy

Cells were attached to poly-L-Lysine-coated coverslips and fixed with 4% paraformaldehyde for 15 min, followed by permeabilization with 0.2% Triton-X 100 in PBS for 15 min, and then blocked with 5% BSA in PBS for 1 h at 37 °C. After incubation with primary antibodies overnight at 4 °C, subsequently followed by washing and incubation with appropriate secondary antibodies, confocal images were captured using a laser-scanning confocal microscope (Leica STELLARIS 8, Germany). Images were analyzed using LAS X software.

## Real-time reverse transcription polymerase chain reaction (qRT-PCR)

qRT-PCR analysis was performed to determine the viral loads. Total RNA was extracted from the culture supernatants of cells infected with CCHFV at different time points using TRIzol reagent (Takara, Kusatsu,

Japan) according to the manufacturer's instructions. One-step qRT-PCR was used to determine the viral loads using a One-Step PrimeScript™ RT-PCR Kit (Takara) and a StepOnePlus Real-Time PCR System (Applied Biosystems, Foster City, CA, USA). The primer pairs used in this study were as follows: *hifitm3* forward: 5′-AATCACACTGTCCAAACCT-3′, and reverse: 5′-CTCCTCCTTGAGCATCTC-3′; glyceraldehyde-3-phosphate dehydrogenase (GAPDH) forward: 5′-CAAGGGCATCCTGGGCTACACT-3′, and reverse 5′-CCCAGCGTCAAAGGTGGAGGA-3′; CCHFV NP forward: 5′-TCAAGTGGAGGAARGACATAGG-3′, reverse: 5′-TCCACATGTTCAC GGCTSACTGGG-3′, and the probe: FAM-TCATCRCCACCTCTGTTG AGAA-BHQ1 (Zhang, Y. et al., 2018).

## Generation of IFITM3-overexpressed cell lines and IFITM3-knockout cell lines

MEG-01 and HEK293 cells overexpressing IFITM3 were generated. The *hifitm3* gene was amplified from HeLa cells of human origin and verified by Sanger sequencing. Subsequently, the fragment EGFP-P2A-*hifitm3* was cloned into pLVX-IRES-Puro to generate a recombinant plasmid expressing IFITM3, which was then transferred into HEK293T cells together with the packaging plasmid psPAX2 and skeleton plasmid pMD2.0G at a ratio of 2:1.5:0.5, as previously described (Chang et al., 2024). The supernatant was collected 24 and 48 h after transfection and centrifuged at 1000 ×*g* for 10 min to remove cell debris. HEK293 and MEG-01 cells ($1 \times 10^5$ cells/well) were pre-inoculated into 6-well plates and transduced with the supernatant. After 4 h of transduction, the supernatant was replaced with fresh medium. The overexpression of IFITM3 in cells was examined by flow cytometry and Western blotting.

To generate knockout-hifitm3 MEG-01 (MEG-01-*hifitm3*-KO) and HeLa (HeLa-*hifitm3*-KO) cell lines, the first exon of the human *ifitm3*gene sgRNA or the control sgRNA without a human genome target was cloned into lentiCRISPR v.2 (Addgene, catalog no. 52961). The lentiCRISPR plasmid with the inserted sgRNA, psPAX2 packaging vector, and skeleton plasmid pMD2.0G were co-transfected into HEK293T cells as described above. MEG-01 and HeLa cells were transduced using transfection supernatants and maintained as described above. MEG-01 and HeLa cells were treated with 3 μg/mL and 2 μg/mL puromycin, respectively, after 2 d of expression of selected sgRNA and Cas9 in a 6-well plate. The two most effective IFITM3-targeting sgRNAs were sgRNA1 5′-TTGAG-CATCTCATAGTTGGG-3′ and sgRNA2, 5′-GCAGCAGGGTTCATGAAGA-3′. Gene knockouts were characterized by tracking indels using decomposition (TIDE) analysis. After three rounds of puromycin selection, the genomic DNA was purified using a FastPure Blood/Cell/Tissue/Bacteria DNA Isolation Mini Kit (DC112-01, Vazyme, China). The cell DNA was re-suspended in 200 μL of solution, and PCR was performed as follows: initial denaturation at 95 °C for 3 min, followed by 30 cycles of denaturation at 95 °C for 15 s, annealing at 56 °C for 15 s, and extension at 72 °C for 30 s. The ifitm3 locus was amplified using the following primers: forward 5′-ACCATCCCAGTAACCCACCG-3′ and reverse 5′-GCTGATA-CAGGACTCGGCTCC-3′.

## Pull-down assay

HEK293T cells were co-transfected with two expression plasmids expressing enhanced green fluorescent protein (EGFP)-fused IFITM3 and S-tag-fused viral proteins. At 24 h post-transfection, cells were collected, washed twice with cold PBS, and lysed in immunoprecipitation (IP) lysis buffer (P0013, Beyotime, China) for 30 min on ice. Lytic supernatants were isolated by covalent coupling with anti-EGFP (Abclonal, Wuhan, China) or anti-S-tag single-molecule nanoantibody beads for 4 h at 4 °C to isolate the immune complexes. The beads were washed three times with cold lysis buffer and cold PBS before IP. The precipitated complexes were re-suspended in 1 × SDS loading buffer, separated by SDS-PAGE, and immunoblotted using specific antibodies.

## CCHFV binding and internalization assays

Pre-chilled MEG-01 and MEG-01-*hifitm3*-OE cells were incubated with CCHFV at 4 °C for 1 h, as previously described (Chang et al., 2024). The cells were then washed three times with ice-cold PBS to remove unbound viruses. Viral RNA copy numbers were determined by qRT-PCR. To assess internalized virus loads, cells were further incubated at 37 °C for 1 h after the initial 4 °C incubation. Cells were harvested at specific time points, washed with PBS containing 500 ng/mL proteinase K to remove surface-bound viruses, and used for RNA extraction (Liu et al., 2019). Viral RNA loads were determined using qRT-PCR.

## Plasmid construction and transfection

For intracellular localization and interaction analysis, the human *ifitm3* gene (Genbank accession: NM_021034.3) and the domains including the N-terminal domain (NTD), intramembrane-intracellular loop domain (IMD-CIL), and intracellular loop-transmembrane domain (CIL-TMD) were cloned into the pEGFP-N1 vector fused with EGFP at the C-terminus according to the previous study (Du et al., 2024). The CCHFV encoding Gc fused with S-tag at the C-terminus was constructed into a phCMV vector. All plasmids were verified using Sanger sequencing. Transfection assays were performed with these plasmids using the Lipofectamine 3000 transfection reagent (L3000015, Invitrogen, Thermo Fisher Scientific) according to the manufacturer's instructions.

## Structure prediction

Protein structure models of the human IFITM3 and Gc complexes were predicted using the AlphaFold3 web server (https://golgi.sandbox.google.com/) (Abramson et al., 2024). The salt-bridge and hydrogen-bonding networks were calculated using PDBePISA v1.52 (Krissinel and Henrick, 2007).

## Statistical analysis

All experiments were repeated at least three times unless otherwise stated. Statistical analyses were performed using R (version 4.2.3) and Prism (version 8.0; GraphPad Software, CA, USA) with custom scripts. Differences between two groups were analyzed using a two-tailed unpaired *t*-test, and comparisons among multiple groups were made using a one-way ANOVA. Statistical significance was set at $P < 0.05$.

## DATA AVAILABILITY

All data generated in this study are included in the manuscript.

## ETHICS STATEMENT

The animal study was approved by the Ethics Committee and Biosafety Committee of the Wuhan Institute of Virology, Chinese Academy of Sciences, and was conducted in accordance with the guidelines for the protection of animal subjects (approval number: WIVA33202107).

## AUTHOR CONTRIBUTIONS

Jingyuan Zhang: investigation, methodology, formal analysis, visualization, and writing of the original draft; Yaohui Fang: investigation, methodology, and formal analysis; Chenhui Lin: investigation; Shu Shen: conceptualization, writing review, editing, and supervision; Fei Deng: conceptualization, resources, and supervision.

## CONFLICT OF INTEREST

All authors declare no competing interests. Prof. Fei Deng is an editorial board member for *Virologica Sinica* and was not involved in the editorial review or the decision to publish this article.

## ACKNOWLEDGEMENTS

We thank Mr. Ding Gao, Ms. Anna Du, Ms. Juan Min, Ms. Pei Zhang, and Ms. Bichao Xu from the Core and Technical Support Facilities of the Wuhan Institute of Virology for their assistance. We thank Mr. Jia Wu, Mr. Hao Tang, and Mr. Jun Liu from the BSL-3 Laboratory of Wuhan Institute of Virology team for their critical support with experimental activities and Ms. Min Zhou and Mr. Zhong Zhang for their help with cell culture.

This work was supported by the the National Key R&D Program of China (2024YFC2310000) the Key Project of Key Laboratory of Virology and Biosafety in the Wuhan Institute of Virology, Chinese Academy of Sciences (2024JZZD-02), the Youth Project of the Wuhan Institute of Virology, Chinese Academy of Sciences (2023QNTJ-03), the "Open Competition for Selecting the Best Candidates" Project of the Wuhan East Lake New Technology Development Zone (2022KJB117), the Natural Science Foundation of Hubei Province (2024AFB986), and the Medical Science Research Project of Wuhan Health Commission (WX23B09).

## APPENDIX A. SUPPLEMENTARY DATA

Supplementary data to this article can be found online at https://doi.org/10.1016/j.virs.2025.05.002.

## REFERENCES

Abramson, J., Adler, J., Dunger, J., Evans, R., Green, T., Pritzel, A., Ronneberger, O., Willmore, L., Ballard, A.J., Bambrick, J., et al., 2024. Accurate structure prediction of biomolecular interactions with AlphaFold 3. Nature 630, 493–500.

Akinci, E., Bodur, H., Leblebicioglu, H., 2013. Pathogenesis of Crimean-Congo hemorrhagic fever. Vector Borne Zoonotic Dis. 13, 429–437.

Akinci, E., Bodur, H., Sunbul, M., Leblebicioglu, H., 2016. Prognostic factors, pathophysiology and novel biomarkers in Crimean-Congo hemorrhagic fever. Antivir. Res. 132, 233–243.

Aligholipour Farzani, T., Foldes, K., Hanifehnezhad, A., Yener Ilce, B., Bilge Dagalp, S., Amirzadeh Khiabani, N., Ergunay, K., Alkan, F., Karaoglu, T., Bodur, H., Ozkul, A., 2019. Bovine herpesvirus type 4 (BoHV-4) vector delivering nucleocapsid protein of crimean-Congo hemorrhagic fever virus induces comparable protective immunity against lethal challenge in IFNalpha/beta/gammaR-/- mice models. Viruses 11, 237.

Aslam, M., Abbas, R.Z., Alsayeqh, A., 2023. Distribution pattern of Crimean-Congo hemorrhagic fever in Asia and the Middle East. Front. Public Health 11, 1093817.

Bailey, C.C., Kondur, H.R., Huang, I.C., Farzan, M., 2013. Interferon-induced transmembrane protein 3 is a type II transmembrane protein. J. Biol. Chem. 288, 32184–32193.

Bailey, C.C., Zhong, G., Huang, I.C., Farzan, M., 2014. IFITM-family proteins: the cell's first line of antiviral defense. Annu. Rev. Virol. 1, 261–283.

Bente, D.A., Forrester, N.L., Watts, D.M., Mcauley, A.J., Whitehouse, C.A., Bray, M., 2013. Crimean-Congo hemorrhagic fever: history, epidemiology, pathogenesis, clinical syndrome and genetic diversity. Antivir. Res. 100, 159–189.

Bodur, H., Akinci, E., Ascioglu, S., Onguru, P., Uyar, Y., 2012. Subclinical infections with Crimean-Congo hemorrhagic fever virus, Turkey. Emerg. Infect. Dis. 18, 640–642.

Bote, J., Corkrey, H.A., Koupenova, M., 2022. Human platelets and influenza virus: internalization and platelet activation. Platelets 33, 184–191.

Brass, A.L., Huang, I.C., Benita, Y., John, S.P., Krishnan, M.N., Feeley, E.M., Ryan, B.J., Weyer, J.L., Van Der Weyden, L., Fikrig, E., Adams, D.J., Xavier, R.J., Farzan, M., Elledge, S.J., 2009. The IFITM proteins mediate cellular resistance to influenza A H1N1 virus, West Nile virus, and dengue virus. Cell 139, 1243–1254.

Campbell, R.A., Schwertz, H., Hottz, E.D., Rowley, J.W., Manne, B.K., Washington, A.V., Hunter-Mellado, R., Tolley, N.D., Christensen, M., Eustes, A.S., et al., 2019. Human megakaryocytes possess intrinsic antiviral immunity through regulated induction of IFITM3. Blood 133, 2013–2026.

Chang, M., Min, Y.Q., Xu, Z., Deng, F., Wang, H., Ning, Y.J., 2024. Host factor MxA restricts Dabie bandavirus infection by targeting the viral NP protein to inhibit NP-RdRp interaction and ribonucleoprotein activity. J. Virol. 98, e0156823.

Chen, H., Jie, C., Tang, L.P., Meng, H., Li, X.B., Li, Y.B., Chen, L.X., Yan, C., Kurihara, H., Li, Y.F., He, R.R., 2017. New insights into the effects and mechanism of a classic traditional Chinese medicinal formula on influenza prevention. Phytomedicine 27, 52–62.

Chumakov, M.P., Butenko, A.M., Shalunova, N.V., Mart'ianova, L.I., Smirnova, S.E., Bashkirtsev Iu, N., Zavodova, T.I., Rubin, S.G., Tkachenko, E.A., Karmysheva, V., Reingol'd, V.N., Popov, G.V., Savinov, A.P., 1968. [New data on the viral agent of Crimean hemorrhagic fever]. Vopr. Virusol. 13, 377.

Compton, A.A., Roy, N., Porrot, F., Billet, A., Casartelli, N., Yount, J.S., Liang, C., Schwartz, O., 2016. Natural mutations in IFITM3 modulate post-translational regulation and toggle antiviral specificity. EMBO Rep. 17, 1657–1671.

Cross, R.W., Prasad, A.N., Borisevich, V., Geisbert, J.B., Agans, K.N., Deer, D.J., Fenton, K.A., Geisbert, T.W., 2020. Crimean-Congo hemorrhagic fever virus strains Hoti and Afghanistan cause viremia and mild clinical disease in cynomolgus monkeys. PLoS Neglected Trop. Dis. 14, e0008637.

Dai, S., Wu, Q., Wu, X., Peng, C., Liu, J., Tang, S., Zhang, T., Deng, F., Shen, S., 2021. Differential cell line susceptibility to crimean-Congo hemorrhagic fever virus. Front. Cell. Infect. Microbiol. 11, 648077.

Denz, P.J., Speaks, S., Kenney, A.D., Eddy, A.C., Papa, J.L., Roettger, J., Scace, S.C., Rubrum, A., Hemann, E.A., Forero, A., Webby, R.J., Bowman, A.S., Yount, J.S., 2024. Innate immune control of influenza virus interspecies adaptation via IFITM3. Nat. Commun. 15, 9375.

Deyde, V.M., Khristova, M.L., Rollin, P.E., Ksiazek, T.G., Nichol, S.T., 2006. Crimean-Congo hemorrhagic fever virus genomics and global diversity. J. Virol. 80, 8834–8842.

Dib, P.R.B., Quirino-Teixeira, A.C., Merij, L.B., Pinheiro, M.B.M., Rozini, S.V., Andrade, F.B., Hottz, E.D., 2020. Innate immune receptors in platelets and platelet-leukocyte interactions. J. Leukoc. Biol. 108, 1157–1182.

Du, S., Wang, Y., Wang, J., Ma, Y., Xu, W., Shi, X., Li, L., Hao, P., Liu, Q., Liao, M., Zhou, B., Jin, N., Wong, Y.K., Hu, L., Wang, J., Liu, W., Li, C., 2024. IFITM3 inhibits severe fever with thrombocytopenia syndrome virus entry and interacts with viral Gc protein. J. Med. Virol. 96, e29491.

Ergonul, O., 2012. Crimean-Congo hemorrhagic fever virus: new outbreaks, new discoveries. Curr Opin Virol 2, 215–220.

Fang, Y., Shen, S., Zhang, J., Xu, L., Wang, T., Fan, L., Zhu, Q., Xiao, J., Wu, X., Jin, J., Wu, Q., Zhang, Y., Tang, S., Zheng, X., Deng, F., 2024. Thrombocytopenia in SFTS due to platelets with altered function undergoing cell death pathways. J. Infect. Dis. 231, e183–e194.

Fereidouni, M., Apanaskevich, D.A., Pecor, D.B., Pshenichnaya, N.Y., Abuova, G.N., Tishkova, F.H., Bumburidi, Y., Zeng, X., Kuhn, J.H., Keshtkar-Jahromi, M., 2023. Crimean-Congo hemorrhagic fever virus in Central, Eastern, and South-eastern Asia. Virol. Sin. 38, 171–183.

Garrison, A.R., Smith, D.R., Golden, J.W., 2019. Animal models for crimean-Congo hemorrhagic fever human disease. Viruses 11, 590.

Guo, R., Shen, S., Zhang, Y., Shi, J., Su, Z., Liu, D., Liu, J., Yang, J., Wang, Q., Hu, Z., Zhang, Y., Deng, F., 2017. A new strain of Crimean-Congo hemorrhagic fever virus isolated from Xinjiang, China. Virol. Sin. 32, 80–88.

Haddock, E., Feldmann, F., Hawman, D.W., Zivcec, M., Hanley, P.W., Saturday, G., Scott, D.P., Thomas, T., Korva, M., Avsic-Zupanc, T., Safronetz, D., Feldmann, H., 2018. A cynomolgus macaque model for Crimean-Congo haemorrhagic fever. Nat. Microbiol. 3, 556–562.

Hoogstraal, H., 1979. The epidemiology of tick-borne Crimean-Congo hemorrhagic fever in Asia, Europe, and Africa. J. Med. Entomol. 15, 307–417.

Jia, R., Pan, Q., Ding, S., Rong, L., Liu, S.L., Geng, Y., Qiao, W., Liang, C., 2012. The N-terminal region of IFITM3 modulates its antiviral activity by regulating IFITM3 cellular localization. J. Virol. 86, 13697–13707.

Klein, S., Golani, G., Lolicato, F., Lahr, C., Beyer, D., Herrmann, A., Wachsmuth-Melm, M., Reddmann, N., Brecht, R., Hosseinzadeh, M., Kolovou, A., Makroczyova, J., Peterl, S., Schorb, M., Schwab, Y., Brugger, B., Nickel, W., Schwarz, U.S., Chlanda, P., 2023. IFITM3 blocks influenza virus entry by sorting lipids and stabilizing hemifusion. Cell Host Microbe 31, 616–633 e620.

Koupenova, M., Livada, A.C., Morrell, C.N., 2022. Platelet and megakaryocyte roles in innate and adaptive immunity. Circ. Res. 130, 288–308.

Krissinel, E., Henrick, K., 2007. Inference of macromolecular assemblies from crystalline state. J. Mol. Biol. 372, 774–797.

Li, Y., Zhang, J., Liu, X., Zhang, X., Shi, G., 2025. Identification of IFITM3 as a diagnostic biomarker of systemic lupus erythematosus and its association with disease activity based on multi-omics and experimental verification. Lupus 34, 57–70.

Lin, X., Yu, S., Ren, P., Sun, X., Jin, M., 2020. Human microRNA-30 inhibits influenza virus infection by suppressing the expression of SOCS1, SOCS3, and NEDD4. Cell. Microbiol. 22, e13150.

Lindquist, M.E., Zeng, X., Altamura, L.A., Daye, S.P., Delp, K.L., Blancett, C., Coffin, K.M., Koehler, J.W., Coyne, S., Shoemaker, C.J., Garrison, A.R., Golden, J.W., 2018. Exploring Crimean-Congo hemorrhagic fever virus-induced hepatic injury using antibody-mediated type I interferon blockade in mice. J. Virol. 92, e01083-18.

Liu, J., Xu, M., Tang, B., Hu, L., Deng, F., Wang, H., Pang, D.W., Hu, Z., Wang, M., Zhou, Y., 2019. Single-particle tracking reveals the sequential entry process of the bunyavirus severe fever with thrombocytopenia syndrome virus. Small 15, e1803788.

Lu, J., Pan, Q., Rong, L., He, W., Liu, S.L., Liang, C., 2011. The IFITM proteins inhibit HIV-1 infection. J. Virol. 85, 2126–2137.

Machlus, K.R., Italiano Jr., J.E., 2013. The incredible journey: from megakaryocyte development to platelet formation. J. Cell Biol. 201, 785–796.

Marziali, F., Delpeuch, M., Kumar, A., Appourchaux, R., Dufloo, J., Tartour, K., Etienne, L., Cimarelli, A., 2021. Functional heterogeneity of mammalian IFITM proteins against HIV-1. J. Virol. 95, e0043921.

Mcentire, C.R.S., Song, K.W., Mcinnis, R.P., Rhee, J.Y., Young, M., Williams, E., Wibecan, L.L., Nolan, N., Nagy, A.M., Gluckstein, J., Mukerji, S.S., Mateen, F.J., 2021. Neurologic manifestations of the world Health organization's list of pandemic and epidemic diseases. Front. Neurol. 12, 634827.

Mo, Q., Feng, K., Dai, S., Wu, Q., Zhang, Z., Ali, A., Deng, F., Wang, H., Ning, Y.J., 2023. Transcriptome profiling highlights regulated biological processes and type III

interferon antiviral responses upon Crimean-Congo hemorrhagic fever virus infection. Virol. Sin. 38, 34–46.
Narayana, S.K., Helbig, K.J., Mccartney, E.M., Eyre, N.S., Bull, R.A., Eltahla, A., Lloyd, A.R., Beard, M.R., 2015. The interferon-induced transmembrane proteins, IFITM1, IFITM2, and IFITM3 inhibit hepatitis C virus entry. J. Biol. Chem. 290, 25946–25959.
Neogi, U., Elaldi, N., Appelberg, S., Ambikan, A., Kennedy, E., Dowall, S., Bagci, B.K., Gupta, S., Rodriguez, J.E., Svensson-Akusjarvi, S., Monteil, V., Vegvari, A., Benfeitas, R., Banerjea, A., Weber, F., Hewson, R., Mirazimi, A., 2022. Multi-omics insights into host-viral response and pathogenesis in Crimean-Congo hemorrhagic fever viruses for novel therapeutic target. eLife 11, e76071.
Quirino-Teixeira, A.C., Andrade, F.B., Pinheiro, M.B.M., Rozini, S.V., Hottz, E.D., 2022. Platelets in dengue infection: more than a numbers game. Platelets 33, 176–183.
Ren, L., Du, S., Xu, W., Li, T., Wu, S., Jin, N., Li, C., 2020. Current progress on host antiviral factor IFITMs. Front. Immunol. 11, 543444.
Schoggins, J.W., Wilson, S.J., Panis, M., Murphy, M.Y., Jones, C.T., Bieniasz, P., Rice, C.M., 2011. A diverse range of gene products are effectors of the type I interferon antiviral response. Nature 472, 481–485.
Scholte, F.E.M., Zivcec, M., Dzimianski, J.V., Deaton, M.K., Spengler, J.R., Welch, S.R., Nichol, S.T., Pegan, S.D., Spiropoulou, C.F., Bergeron, E., 2017. Crimean-Congo hemorrhagic fever virus suppresses innate immune responses via a ubiquitin and ISG15 specific protease. Cell Rep. 20, 2396–2407.
Shtanko, O., Nikitina, R.A., Altuntas, C.Z., Chepurnov, A.A., Davey, R.A., 2014. Crimean-Congo hemorrhagic fever virus entry into host cells occurs through the multivesicular body and requires ESCRT regulators. PLoS Pathog. 10, e1004390.
Simon, A.Y., Sutherland, M.R., Pryzdial, E.L., 2015. Dengue virus binding and replication by platelets. Blood 126, 378–385.
Tartour, K., Appourchaux, R., Gaillard, J., Nguyen, X.N., Durand, S., Turpin, J., Beaumont, E., Roch, E., Berger, G., Mahieux, R., Brand, D., Roingeard, P., Cimarelli, A., 2014. IFITM proteins are incorporated onto HIV-1 virion particles and negatively imprint their infectivity. Retrovirology 11, 103.
Tignor, G.H., Hanham, C.A., 1993. Ribavirin efficacy in an in vivo model of Crimean-Congo hemorrhagic fever virus (CCHF) infection. Antivir. Res. 22, 309–325.
Tipih, T., Meade-White, K., Rao, D., Bushmaker, T., Lewis, M., Shaia, C., Feldmann, H., Hawman, D.W., 2023. Favipiravir and Ribavirin protect immunocompetent mice from lethal CCHFV infection. Antivir. Res. 218, 105703.
Xu, W., Wang, Y., Li, L., Qu, X., Liu, Q., Li, T., Wu, S., Liao, M., Jin, N., Du, S., Li, C., 2022. Transmembrane domain of IFITM3 is responsible for its interaction with influenza virus HA(2) subunit. Virol. Sin. 37, 664–675.
Yao, L., Dong, H., Zhu, H., Nelson, D., Liu, C., Lambiase, L., Li, X., 2011. Identification of the IFITM3 gene as an inhibitor of hepatitis C viral translation in a stable STAT1 cell line. J. Viral Hepat. 18, e523–e529.
Zani, A., Yount, J.S., 2018. Antiviral protection by IFITM3 in vivo. Curr. Clin. Microbiol. Rep. 5, 229–237.
Zhang, P., Ruan, C., Yang, G., Guan, Y., Zhu, Y., Li, Q., Dai, X., An, Y., Shi, X., Huang, P., Chen, Y., He, Z., Du, Z., Liu, C., 2024. PGRN inhibits early B-cell activation and IgE production through the IFITM3-STAT1 signaling pathway in asthma. Adv. Sci. (Weinh.) 11, e2403939.
Zhang, Y., Shen, S., Fang, Y., Liu, J., Su, Z., Liang, J., Zhang, Z., Wu, Q., Wang, C., Abudurexiti, A., Hu, Z., Zhang, Y., Deng, F., 2018. Isolation, characterization, and phylogenetic analysis of two new Crimean-Congo hemorrhagic fever virus strains from the Northern region of Xinjiang Province, China. Virol. Sin. 33, 74–86.
Zivcec, M., Safronetz, D., Scott, D., Robertson, S., Ebihara, H., Feldmann, H., 2013. Lethal Crimean-Congo hemorrhagic fever virus infection in interferon alpha/beta receptor knockout mice is associated with high viral loads, proinflammatory responses, and coagulopathy. J. Infect. Dis. 207, 1909–1921.